Environmental Science & Technology

Article

Cite This: Environ. Sci. Technol. 2019, 53, 6708−6717

pubs.acs.org/est

Effect of Oxalate and Sulfate on Iron-Catalyzed Secondary Brown Carbon Formation

Aseel Al Nimer,[†,#] Laura Rocha,[†,#] Mohammad A. Rahman,[†] Sergey A. Nizkorodov,[‡] and Hind A. Al-Abadleh*[,†]

[†]Department of Chemistry and Biochemistry, Wilfrid Laurier University, Waterloo, ON N2L 3C5, Canada

[‡]Department of Chemistry, University of California, Irvine, CA 92697, United States

Supporting Information

ABSTRACT: Oxalate and sulfate are ubiquitous components of ambient aerosols with a high complexation affinity to iron. However, their effect on iron-driven secondary brown carbon formation in solution from soluble aromatic and aliphatic reagents was not studied. We report masses and hydrodynamic particle sizes of insoluble particles formed from the dark aqueous phase reaction of catechol, guaiacol, fumaric, and muconic acids with Fe(III) in the presence of oxalate or sulfate. Results show that oxalate decreases particle yield in solution from the reaction of Fe(III), with a stronger effect for guaiacol than catechol. For both compounds, the addition of sulfate results in the formation of more polydisperse (0.1−5 μm) and heavier particles than those from control experiments. Reactions with fumaric and muconic acids show that oxalate (not sulfate) and pH are determining factors in the efficiency of particle formation in solution. Polymerization reactions occur readily in the presence of sulfate in solution producing particles with iron-coordinated and/or pore-trapped sulfate anions. The addition of oxalate to the reactions of Fe(III) with all organics, except guaiacol, produced fewer and larger polymeric particles (>0.5 μm). These results imply that even in the presence of competing ligands, the formation of insoluble and colored particles from soluble organic precursors still dominates over the formation of soluble iron complexes.

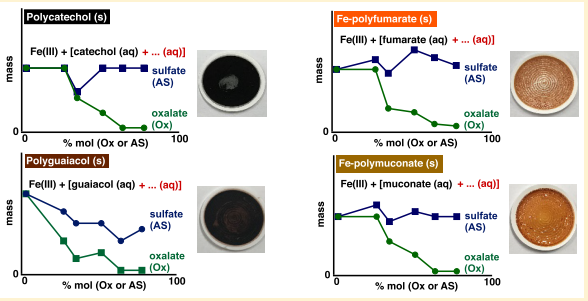

INTRODUCTION

The formation of atmospheric particulate matter from precursor gases is an active area of research. Our understanding of secondary organic aerosol (SOA) formation[1−4] that is being incorporated in global climate models[5] is based on processes that include atmospheric oxidation of volatile organic compounds (VOCs) from biogenic and anthropogenic sources, gas-particle partitioning, and multiphase/heterogeneous reactions. Chemical and photochemical aging processes that take place following the initial SOA formation may produce light-absorbing soluble and insoluble components collectively known as "brown carbon".[6] Despite the high level of activity in this research area, the role of transition metals such as iron in the formation and aging of SOA and brown carbon in the aqueous phase, such as cloud/fog droplets and deliquesced aerosol particles, is still poorly known.[7] Various iron compounds have been identified in mineral dust, fly ash, and marine aerosols.[8−12] During long-range transport, the fraction of soluble iron in particles is enhanced due to uptake of acidic gases[12−15] and dissolved organic matter.[16] In addition, cycling between wet aerosols, characterized by highly acidic conditions, and cloud droplets, characterized by more pH-neutral conditions, affects the concentration of soluble iron in the particles.[14,17−20]

Soluble iron is known to catalyze a number of redox and photochemical reactions that change the inorganic and organic composition of atmospheric particles. For example, Fe(II)/Fe(III) species are well-known to catalyze the formation of sulfate species, hydroxyl, and organic peroxy radicals via Fenton and photo Fenton chemistry.[7] The mechanisms of particle phase reactions involving Fe(II)/Fe(III) depend on aerosol pH and liquid water content.[21,22] In addition, certain organic ligands can affect the reaction mechanisms or directly participate in redox chemistry.[23,24] For example, biomass burning processes produce phenolic compounds,[6] which are known to complex to Fe efficiently and may therefore affect its chemistry in iron-containing particles. Aged SOA particles containing water-soluble dicarboxylic acids may also come in contact with processed iron-containing aerosols during long-range transport.[25] These interactions will not only change the mixing state of the aerosol, but soluble iron will catalyze reactions that change the chemical composition and size of these particles. The investigation of bulk phase reactions between soluble iron species and water-soluble organic compounds is relevant to our understanding of aerosol aging processes, as well as processes occurring in cloud and fog droplets.

Received: January 14, 2019
Revised: April 27, 2019
Accepted: April 29, 2019
Published: April 29, 2019

DOI: 10.1021/acs.est.9b00237
Environ. Sci. Technol. 2019, 53, 6708−6717

We recently reported that Fe(III) in aqueous solution leads to the formation of secondary brown carbon via oxidative polymerization of water-soluble polyphenols and metal-catalyzed polymerization of water-soluble dicarboxylic acids in the pH range 3−5.[23,24] The light absorption by the polyphenolic polymers (polycatechol and polyguaiacol) arises from the conjugated aromatic network.[23] Ligand-to-metal-charge transfer (LMCT) explains the browning of iron-coordinated organometallic polymers (Fe-polyfumarate and Fe-polymuconate).[24] Despite the difference in the mechanism of light absorption and the presence of Fe in Fe-polyfumarate and Fe-polymuconate, we will refer to both types of polymer as different examples of brown carbon. These aqueous phase reactions with Fe(III) were studied under high solute to solvent ratio to mimic reactions in adsorbed water.[23] Also, the pH range in our experiments matches that of ambient aerosols collected in field campaigns such as MILAGRO and the China-Haze event.[21,26] In the course of this work, polycatechol and polyguaiacol were found to be insoluble at neutral and acidic pH. At basic pH (∼12−13), polyguaiacol became soluble. Iron-coordinated organometallic polymers were found to be insoluble regardless of pH. The poor solubility of these materials distinguishes them from oligomeric compounds formed during VOC oxidation and SOA aging, which are largely water-soluble.[27]

Oxalate and sulfate are ubiquitous components of ambient aerosols with a high complexation affinity to iron. The work by Kundu et al. on biomass burning aerosols showed that 77% of oxalic acid is formed from degradation of dicarboxylic acids and related compounds and 23% are likely directly emitted or chemically produced from other unknown precursors.[28] Other well-studied mechanisms of oxalate formation in atmospheric aqueous particles are the oxidations of glyoxal and methylglyoxal.[29] Recently, Zhang et al. reported results from field measurements showing enhanced formation of oxalate associated with Fe-containing particles.[30] They attributed this observation to complexation of oxalate to iron following gas-particle partitioning of oxalic acid. In general, aqueous phase oxalate is the most effective organic compound among the known atmospheric organic binding ligands that promotes dust iron solubility.[31] Sulfate is one of the most abundant inorganic components in aerosols that is mainly formed from aqueous phase oxidation of SO_2, a process that is often catalyzed by soluble iron.[32] Sulfate is routinely measured and incorporated in thermodynamic models that calculate aerosol pH.[33] Yu et al. reported a correlation between the sulfate and oxalate contents in particles and suggested a dominant in-cloud processing pathway to explain the close tracking of both species.[34] Nonsea-salt sulfate (nss SO_4^{2-}) from anthropogenic sources was also reported to largely control the formation of water-soluble SOA dominated by oxalate via aqueous phase photochemical reactions.[35]

Our previous experiments focused on aqueous phase reactions between Fe(III) and catechol, guaiacol, fumaric acid, and muconic acid in solutions that did not contain oxalate or sulfate. The objective of this study is to investigate the competing effects of the additions of oxalate and sulfate on the efficiency of insoluble particle formation from the dark aqueous phase reaction of iron with the same organic reagents. Specifically, we quantified the mass of insoluble products as a function of pH and concentrations of oxalate and sulfate. Average hydrodynamic particle size was studied in situ using dynamic light scattering (DLS). The results were compared to those in control solutions with no added oxalate or sulfate. The implications of these investigations are discussed in the context of new pathways for insoluble SOA and brown carbon formation in solution driven by soluble iron species and the factors that affect the efficiency of these pathways.

MATERIALS AND METHODS

Chemicals. All chemicals were used as received without further purification. More details on the sources, purity, and description of solution preparations are provided in the Supporting Information (SI).

Product Mass Experiments. Particles that formed in 20 mL of solution after a 2 h reaction between $FeCl_3$ and organic reagents in the absence and presence of oxalate and sulfate were collected on preweighed nylon membrane filters (0.2 μm pore size, 25 mm dia., EMD), and the filters were dried and weighed. To investigate the effect of iron speciation shown in Figure S1 on particle formation in solution, two experimental methods were performed. In *method 1*, the organic reagent was first mixed with either oxalate or sulfate for a few minutes, then the reaction was started by the addition of $FeCl_3$ solution. In *method 2*, either oxalate or sulfate was mixed with the $FeCl_3$ solution for 2 h, then the organic reagent was added for an additional 2 h. *Method 1* explores the reactivity of the iron hydroxide species dominant at pH 3 and 5 with the organic ligands in solution, whereas *method 2* examines the reactivity of soluble iron oxalate and iron sulfate with the soluble organic precursors used herein. While we observed particle formation at shorter times (as low as 1 min),[23,24] the 2 h reaction time was chosen to achieve a measurable mass of the precipitate and to ensure consistency with our previous work. More details are provided in the SI.

Chromatography Experiments. HPLC experiments were performed to quantify the concentration of the soluble organic reagents before and after reaction with $FeCl_3$, in the absence and presence of oxalate and sulfate. In addition, ion chromatography was used to quantify the consumption of sulfate in the formation of polycatechol particles from catechol solutions containing sulfate. More details are provided in the SI.

Dynamic Light Scattering (DLS) Experiments. To monitor the insoluble particle growth in solution as a function of time, DLS experiments were performed on reaction solutions prepared according to *method 1* or *2*. The concentrations used were an order of magnitude smaller than those used for product mass experiments in order to match the dynamic range of the DLS instrument. The reaction took place in a 1 cm disposable cuvette, and the data were collected using a Malvern Zetasizer Nano (ZEN3600). More details are provided in the SI.

Particle Characterization. Solid particles were characterized for the organic functional groups and thermal properties using attenuated total reflection Fourier transform infrared spectroscopy (ATR-FTIR) and thermogravimetric analysis/differential scanning calorimetry (TGA/DSC), respectively. More details are provided in the SI.

RESULTS AND DISCUSSION

1. Effect of Oxalate and Sulfate on Product Mass. The mass values of the insoluble particles produced after 2 h reactions of catechol, guaiacol, fumarate, and muconate with $FeCl_3$ in the presence of oxalate (Ox) and ammonium sulfate

DOI: 10.1021/acs.est.9b00237
Environ. Sci. Technol. 2019, 53, 6708−6717

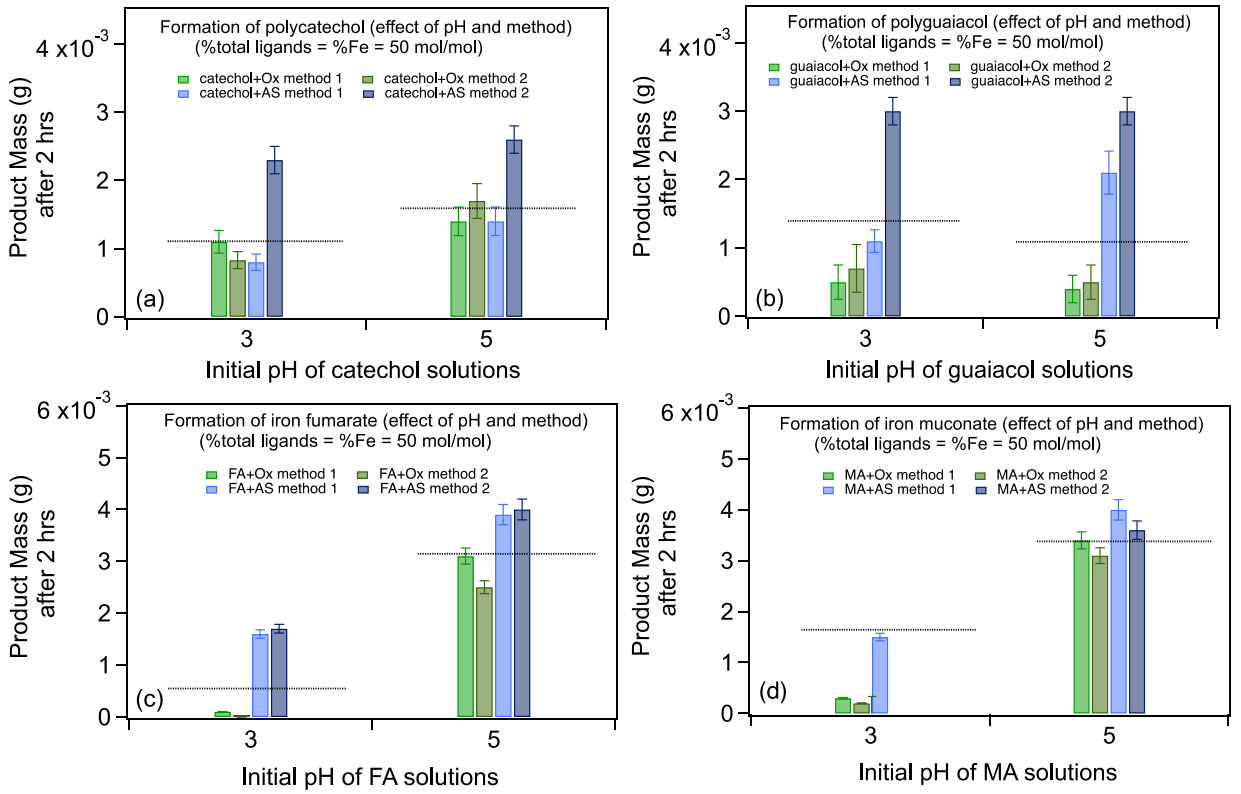

Figure 1. Effect of pH and method on the product mass after 2 h reaction between catechol, guaiacol, fumarate (FA), and muconate (MA) and $FeCl_3$ in the absence and presence of oxalate (Ox) and ammonium sulfate (AS). The concentration of the organic precursor is 1 mM. The dashed lines in the graphs correspond to product mass from control experiments using 2:1 (67.7:33.3% mol/mol) Fe/organic precursor. Error bars represent the average of 2−3 repeated measurements.

(AS) is shown in Figure 1. The produced mass values are plotted as a function of method and pH for the 2:1:1 Fe/organic/Ox or AS. The product mass for the control reactions (no added oxalate or sulfate) is also shown (dashed lines) using a 2:1 Fe/organic reagent under the same experimental conditions. In most cases, the resulting product mass is within the same order of magnitude; however, there are subtle differences based on pH and the method of particle formation in solution. Figure 2 shows how the mass of the insoluble particles depends on the molar ratios between Fe, organic reagent (catechol, guaiacol, fumarate, and muconate), and ligand (oxalate or sulfate) in *method 1* experiments. The protonation states of the organic reagents at a given pH can be inferred from their pK_a values. The following sections describe results obtained using the aromatic reagents and aliphatic dicarboxylic acids.

1a. Reactions of Fe(III) with Catechol and Guaiacol. Catechol (pK_a 9.3 and 12.6 for the first and second ionization steps)[36] and guaiacol (pK_a 9.9)[37] were reacted with $FeCl_3$ in the absence and presence of added oxalate and sulfate. The reaction was carried out at pH 3 for consistency with our earlier work.[23] Figure 2a–d shows the insoluble product mass for different molar ratios of each chemical in solution. Mass yields are ∼50% for catechol and 60% for guaiacol relative to the initial masses of the organics in the starting solution. On average, the maximal yields are observed at the 2:1:1 Fe/organic/Ox or AS molar ratios (the data chosen for Figure 1). Figure S2a,b shows representative photographs of filters containing polycatechol and polyguaiacol from reactions in the presence of oxalate. The yields drop when the ratio deviates from this optimal value in either direction.

The data in Figures 1 and 2 show that oxalate suppressed particle formation from catechol and guaiacol in solution at pH 3 to a larger extent than sulfate, regardless of whether *method 1* or *2* was used. The data also show a larger reduction in particle mass with guaiacol than with catechol. Particle formation in solution from catechol in the presence of iron and dissolved oxygen under acidic conditions occurs via oxidative polymerization that involves multiple steps initiated by the complexation to Fe(III) (Scheme S1).[23,38] At pH 3, the dominant species of $FeCl_3$(aq) is $FeOH^{2+}$ (Figure S1a) and that of oxalate is $HC_2O_4^-$ (pK_{a1} < pH < pK_{a2}). Hence, catechol as a ligand competes with $HC_2O_4^-$ for binding to $FeOH^{2+}$. The logarithms of complexation constants, log *K*, for these reactions are 9.9 and 6.9 (refer to the SI section, reactions S17 and S18), which reflect thermodynamic favorability for the formation of $Fe(C_6O_2H_4)^+$ and $Fe(C_2O_4)^+$, respectively. While catechol is fully protonated at pH 3 (and 5), it is known that iron promotes the deprotonation of polyphenols under acidic conditions forming hydrogen catecholate, $H(C_6O_2H_4)^-$.[39] The higher log *K* value for the $H(C_6O_2H_4)^-$ complexation to $FeOH^{2+}$ explains why the product mass is identical to the control value when both catechol and oxalate are present in equimolar amounts at pH 3 (Figure 2a). When $HC_2O_4^-$ and $FeOH^{2+}$ reacted first for 2 h according to *method 2* at pH 3 (Figure 1a), the product mass was slightly lower than that in Figure 2a when catechol was added with equimolar quantities to oxalate. In this case, favorable ligand exchange between $H(C_6O_2H_4)^-$ and $Fe(C_2O_4)^+$ complexes occurs according to

DOI: 10.1021/acs.est.9b00237
Environ. Sci. Technol. 2019, 53, 6708−6717

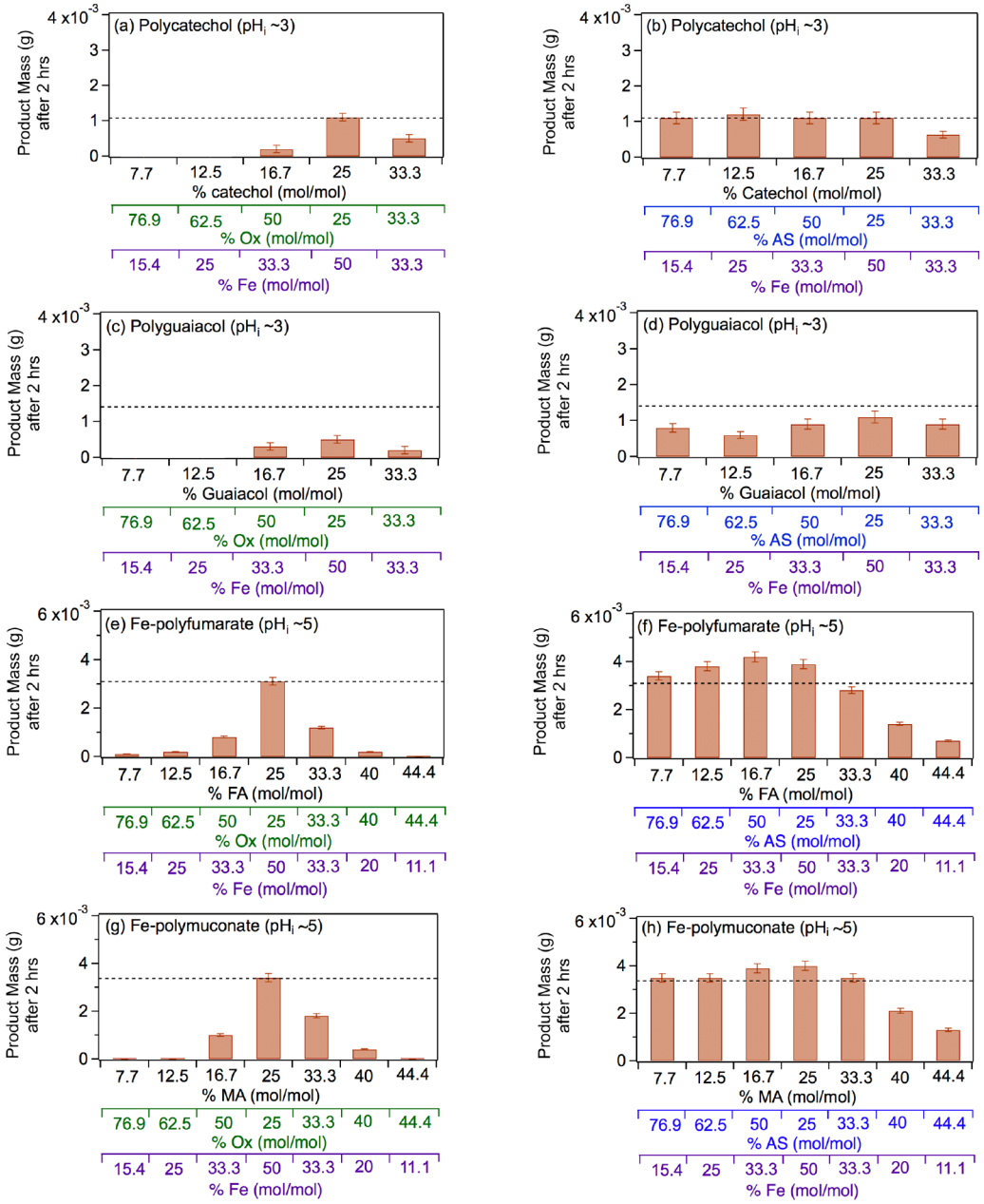

Figure 2. Effect of adding oxalate (Ox, left) and ammonium sulfate (AS, right) on product mass after 2 h dark aqueous phase reaction of 1 mM catechol, guaiacol, fumarate (FA), and muconate (MA) with $FeCl_3$ (total volume = 20 mL) according to *method 1*. The error bars represent the standard deviation ($\pm\sigma$) from averaging 3–4 filter weight values. The horizontal dashed line is the product mass for the control reaction (no added oxalate or sulfate).

reaction S19 with log K = 3. However, when oxalate is present in excess relative to catechol (left side of 2:1:1 Fe/catechol/Ox molar ratio, Figure 2a), the formation of particles in solution is suppressed. This suppression is explained by the predominance of soluble iron oxalate complexes, $Fe(C_2O_4)_2^-$ and $Fe(C_2O_4)_3^{3-}$ (Figure S1b,c and reactions S20 and S21). The log K values for the formation of both complexes equals 8.9, which is much higher than that for the ligand exchange between $H(C_6O_2H_4)^-$ and $Fe(C_2O_4)_2^-$ or $Fe(C_2O_4)_3^{3-}$ (log K = 1, reactions S22 and S23). Particle mass is also lower in the 1:1:1 Fe/catechol/Ox molar ratio (right side of 2:1:1, Figure 2a). This observation is explained by the reduction in the rate of the oxidation polymerization reaction when iron is the limiting reagent relative to catechol as we have shown previously.[23]

In the case of sulfate, the log K value for the formation of soluble iron sulfate, $Fe(SO_4)^+$, 6.3 (reaction S15), is lower than that for $Fe(C_6O_2H_4)^+$ (9.9, reaction S17). These log K values explain the trend in product mass in Figure 2b according to *method 1*, where the addition of sulfate had no effect on particle formation in solution because $FeOH^{2+}$ are still the dominant species in solution (Figure S1d). Under *excess sulfate*, an increase in the concentration of $Fe(SO_4)^+$ relative to $FeOH^{2+}$ species is observed at pH 3 (Figure S1e). Data in Figure 1a show that the product mass is nearly doubled when the reaction resulting in the 2:1:1 Fe/catechol/AS molar ratio is carried out at pH 3 according to *method 2* (i.e., catecholate

DOI: 10.1021/acs.est.9b00237
Environ. Sci. Technol. 2019, 53, 6708–6717

reacts with iron sulfate complexes). Ligand exchange between catecholate and iron sulfate complexes according to reaction S24 is favorable with log K = 3.6. Yet, IC analysis show a 34% reduction in the solution concentration of sulfate following polycatechol formation in solution according to *method 2*. This observation is interpreted in the following sections as the trapping of sulfate within the insoluble paticles, in light of the results from the DLS measurements and particle characterization using ATR-FTIR and TGA/DSC.

To look at the effect of pH on polycatechol formation in solution, the product mass data for catechol in Figure 1a at pH 5 show a slightly higher product mass in the control experiments than that at pH 3 for the 2:1 Fe/catechol molar ratio. At pH 5, the dominant Fe(III) species is $Fe(OH)_2^+$ (Figure S1a).[7] This result is likely due to the higher thermodynamic favorability of soluble complex formation between catecholate and $Fe(OH)_2^+$ species at pH 5 compared to pH 3 (reaction S25 with log K value of 13.7 compared to 9.9 for reaction S17). Within the uncertainty of the measurements, the addition of oxalate in equimolar quantities to catechol, whether according to *method 1 or 2*, does not affect the product mass. The log K value for the formation of soluble iron catecholate complexes is 13.7 (reaction S25), which is lower than that for the formation of soluble iron oxalate (15 in reaction S26). Hence, the formation of soluble iron oxalate complexes is thermodynamically more favorable than that of iron catecholate. Since particles still form using equimolar quantities of oxalate and catechol, this suggests that catecholate binds to the iron oxalate complex by an exchange with water ligands to form an iron oxalate catecholate complex, $Fe(C_2O_4)(C_6O_2H_4)^-$ (see Scheme S2). This complex can form the *o*-quinone necessary for the oxidative polymerization process[23] releasing $Fe(II)(C_2O_4)$ that quickly gets oxidized to $Fe(III)(C_2O_4)^+$ by dissolved oxygen under acidic conditions.[40] The fact that excess oxalate suppresses particle formation in solution, as discussed above, supports this explanation because under these conditions, it is not thermodynamically favorable for catecholate to exchange with oxalate ligands bonded to iron. In the case of sulfate, the results at pH 5 mirror those at pH 3, where no effect on product mass is observed when sulfate is added according to *method 1*, but it is doubled when sulfate is added according to *method 2*.

The mechanism of particle formation in solution from guaiacol is slightly different than that of catechol (Scheme S1). The mechanism involves reduction of Fe(III) to Fe(II) leading to the formation of phenoxy radicals, which then proceeds through C−C radical coupling and further oxidation of the benzene rings.[41−43] Within the uncertainty of the measurements, the addition of oxalate in equimolar quantities to guaiacol at pH 3 suppressed particle formation in solution to a larger extent than that of sulfate (Figure 1c,d). The trend in product mass relative to the control experiments suggests that the efficiency of iron reduction is diminished due to the presence of stable soluble iron oxalate complexes. In the case of iron sulfate, the data in Figure 1b shows that the addition of sulfate according to *method 2* at pH 3 nearly doubled the product mass observed for the control experiments.

For comparison, the mass values of the products at pH 5 shown in Figure 1b with sulfate in solution, whether according to *method 1* or 2, are nearly double that of the control value. At pH 5 and excess iron, $Fe(OH)_2^+$ is the dominant species (Figure S1d) rather than $Fe(SO_4)^+$. As shown in the DLS results and in Particle Characterization below, polyguaiacol particles formed according to *method 2* in the presence of iron sulfate at pH 5 and 3 are more polydisperse than those formed according to *method 1* and they contain residual sulfate. In summary, oxalate decreased particle formation in solution in the reaction of Fe(III) with guaiacol to a larger degree than that with catechol, and the presence of excess iron sulfate appears to incorporate sulfate within the polymeric network.

1b. Reactions of Fe(III) with Fumaric and Muconic Acids. The effects of oxalate and sulfate on product mass in the reactions of soluble aliphatic dicarboxylic acid reagents, fumaric acid (pK_a 3.2, 4.2) and muconic acid (pK_a 3.9, 4.7), with $FeCl_3$ were also investigated. Figure 2e−h shows results as a function of molar ratio at initial pH 5 according to *method 1* for comparison with our earlier work in the absence of oxalate and sulfate.[24] Figure S2c,d shows representative photographs of filters containing Fe-polyfumarate and Fe-polymuconate from reactions in the presence of oxalate. The mass yields are ∼134 ± 13% using fumarate and 110 ± 10% using muconate at pH 5. These yield values are relative to the initial concentrations of the organics in control experiments at pH 5 with no added oxalate or sulfate. These values suggest a polymerization reaction that goes to completion over the 2 h. After accounting for the uncertainty in the mass yield, the higher value for Fe-polyfumarate is explained by the stronger retention of water in the porous structure of this material. These high mass yield values were verified by confirming that the concentration of residual fumarate or muconate in the solution using HPLC was below the detection limit.

The formation of insoluble organometallic polymers using fumarate and muconate is due to metal-catalyzed polymerization of these dicarboxylic acids that involves complexation to Fe(III) (Scheme S3). Neither of these acids have reported values for the log K constant of soluble complex formation. However, the trends in product mass observed in Figure 2e−h can help to infer these log K values. These data show that the product mass for the reaction of 2:1:1 Fe/organic/Ox molar ratio is very close to the control value (no oxalate or sulfate). In addition, the excess oxalate suppresses particle formation in solution from fumarate and muconate at pH 5 to a larger extent than sulfate (left side of the 2:1:1 Fe/organic/Ox molar ratio in Figure 1e,g). These results suggest that the log K values for the formation reactions of soluble iron fumarate and iron muconate are comparable to log K = 15 for the formation of soluble iron oxalate (reaction S26). This log K value is higher than that of reaction S27 between $Fe(OH)_2^+$ and SO_4^{2-} (log K = 10) for the formation of soluble iron sulfate. With comparable log K values for the formation of soluble iron oxalate and iron fumarate/muconate, excess oxalate outcompetes fumarate and muconate in forming much more stable and soluble $Fe(C_2O_4)_2^-$ and $Fe(C_2O_4)_3^{3-}$ (Figure S1c). The log K values for the formations of these complexes are around 21 and 26, respectively (reactions S28 and S29). Hence, excess oxalate suppresses Fe-polyfumarate and Fe-polymuconate particle formation in solution under these conditions. On the basis of the above analysis, a side result of this study is an estimate for the log K range of values to be between 15 and 21 for the formation of iron fumarate/muconate complexes. Excess sulfate does not compete with fumarate because of the higher log K value for soluble iron fumarate formation resulting in product mass values comparable to the control value. The slightly higher product mass results for the experiments with sulfate are explained below. When soluble iron is the limiting reagent (right side of

DOI: 10.1021/acs.est.9b00237
Environ. Sci. Technol. 2019, 53, 6708−6717

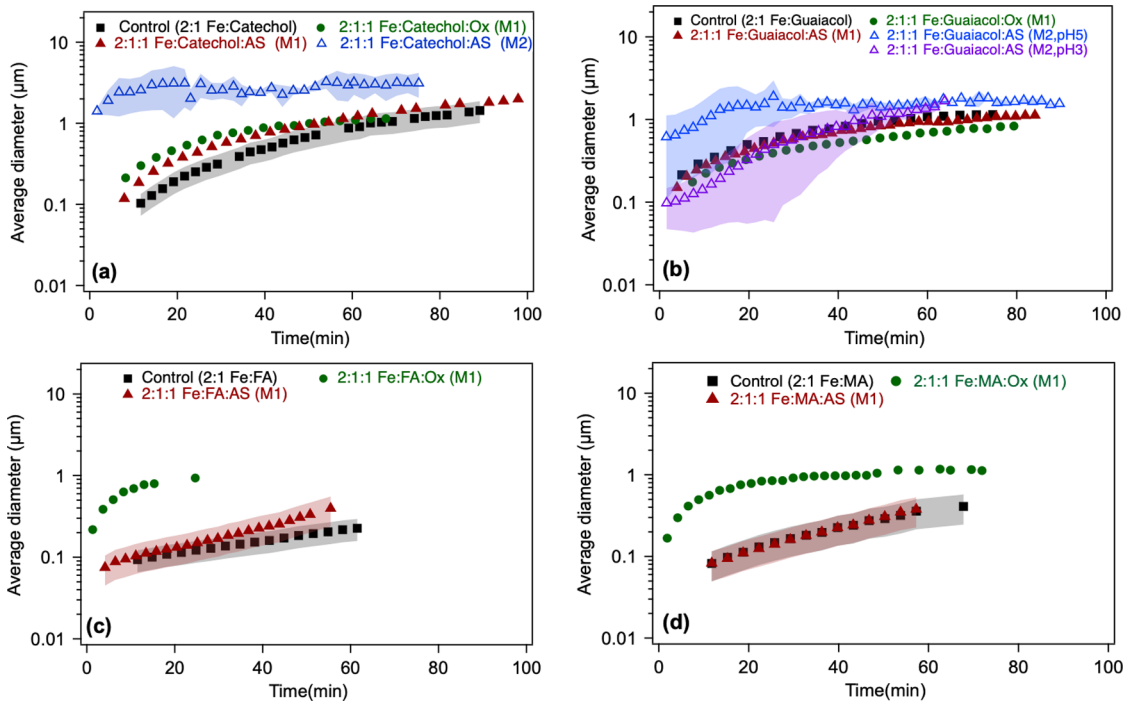

Figure 3. Effect of adding oxalate (Ox) and ammonium sulfate (AS) on particle size from time-dependent DLS measurements during the dark aqueous phase reaction of (a) catechol (1 mM), (b) guaiacol (0.5 mM), and (c) fumarate (50 μM, FA). This molar ratio results in the maximum product mass per data shown in Figure 1. "M1" stands for *method 1*, where organic reagents were mixed first with AS or Ox; reaction time was started when Fe was added. "M2" stands for *method 2*, where AS or Ox were reacted first with Fe for 2 h; reaction time was started when the organic reagent was added. The shaded areas represent the standard deviation of three trials. Unshaded data represent the average of two trials, with a standard deviation the size of the marker width (15%).

the 2:1:1 Fe/organic/Ox/AS molar ratio in Figure 2e,g), the suppression in product mass highlights the central role of excess iron in catalyzing particle formation in solution.

Figure 1c,d shows data that examine the effect of method and initial pH on product mass using the 2:1:1 Fe/organic/Ox/AS molar ratio. Product mass values obtained from reactions conducted according to *method 2* at pH 5 show no significant difference compared to *method 1*, with the exception of oxalate and fumarate. For this system, product mass is lower by a factor of 1.5 when fumarate reacts with iron oxalate complexes according to *method 2*. This result suggests that the formation of soluble iron oxalate complexes prior to the addition of fumarate reduced the amount of available coordination sites on Fe(III) for binding to fumarate, which are necessary for the formation of insoluble Fe-polyfumarate. As for the results at pH 3, which is close to the first pK_a of both fumaric and muconic acids, the product mass values from control experiments (dashed lines) are lower by nearly a factor of 7 and 2, respectively, than at pH 5. The aqueous phase speciation of the organics in solution explains these results. At pH 3, the fully protonated species are dominant for these dicarboxylic acids. Hence, the product mass results suggest that the fully protonated species do not complex with $FeOH^{2+}$ as readily as the fully deprotonated species dominant at pH 5. The addition of oxalate further suppresses particle formation in solution. At pH 3, the dominant species of oxalate is $HC_2O_4^-$, which favorably complexes to $FeOH^{2+}$ with a log K = 6.9 (reaction S18), hence reducing the amount of uncomplexed Fe(III) species for reaction with hydrogen fumarate and muconate species.

The data for polyfumarate in Figures 2f and 1c additionally show significantly higher product mass than the control when sulfate is present at pH 3 and 5, respectively. For comparison, this enhancement in product mass is within the uncertainty of the measurements for polymuconate relative to the control value. As discussed below, the ATR-FTIR results for the dry films of both materials show the presence of sulfate in the solid samples, probably as a result of being trapped in the polymer. In summary, the amount of oxalate (not sulfate), the amount of Fe(III) species relative to the organic reagent, and the protonation states of the aliphatic dicarboxylic acids used herein are determining factors in the efficiency of particle formation in solution. In light of the following sections, the available data suggest that polymerization reactions efficiently take place in the presence or absence of sulfate in solution producing particles with iron-coordinated and/or pore-trapped sulfate groups.

2. Effect of Adding Oxalate or Sulfate on Particle Size of Polymeric Particles. The time-dependent average particle size of polymeric particles produced in situ from the reaction of Fe(III) with aromatic and aliphatic organic reagents in the presence or absence of oxalate (Ox) and sulfate (AS) in solution is shown in Figure 3. Within the first 20 min, the addition of oxalate and sulfate according to *method 1* leads to the formation of polycatechol particles in solution that are 2 and 2.5 times larger than those from the control experiments, respectively (Figure 3a). In light of the product mass yields obtained from filter weighting, one can take the interpretation of the DLS measurements further. For example, since the 2:1:1 Fe/catechol/Ox or AS reaction produces the same product mass as the 2:1 Fe/catechol control (Figure 2a) but the particles are initially larger (Figure 3a), there must be fewer of them in the solution. This can perhaps be interpreted that the initial solution nucleation is retarded by oxalate and sulfate, but

DOI: 10.1021/acs.est.9b00237
Environ. Sci. Technol. 2019, 53, 6708−6717

once particles form, they grow faster. When the reaction is carried out according to *method 2* by using sulfate, the DLS measurements show micron-size particles forming right away (Figure 3a). The DLS signal from these particles did not fit the selection criteria outlined in the SI section, most notably having a PDI above 0.5 indicating their high degree of polydispersity. As detailed above in the Product Mass Experiments section, the product mass from this reaction is double the control value at pH 3 (Figure 1a). Hence, these combined results suggest the formation of larger and heavier particles in solution when iron sulfate is reacted with catechol according to *method 2*.

In the case of guaiacol, particles produced according to *method 1* at pH 3 show no significant difference in size when oxalate or sulfate is added relative to the control (Figure 3b). These conditions produce less product mass than the control per data in Figure 2b. However, the cases that produced twice the product mass when sulfate is added according to *method 2* at pH 5 and 3 produce higher variability in particle size within the first 40 min of reaction time. Similar to the results with catechol, these particles have a PDI above 0.5 indicating their high degree of polydispersity. When these results are combined with product mass results, they suggest the formation of fewer and heavier particles in solution when iron sulfate is reacted with guaiacol according to *method 2*.

The DLS data in Figures 3c and S3 show the effect of the addition of oxalate and sulfate on the particle sizes of Fe-polyfumarate and Fe-polymuconate relative to the control. Oxalate and sulfate were added according to *method 1* at pH 5. Within the variability of the DLS results in Figures 3c and S3, it is clear that sulfate has no significant effect on particle size relative to the control. The addition of oxalate appears to initially produce relatively larger particles that grow to micron-size particles at a faster rate than when sulfate is added or in the case of the control. Since these reaction conditions resulted in product masses close to the control value (Figure 2g,h), it can be concluded that the initial solution nucleation is retarded by oxalate, which produces fewer particles. In summary, in situ particle size measurements using DLS show that in general, the addition of oxalate produced relatively larger and fewer polycatechol, Fe-polyfumarate, and Fe-polymuconate particles than the control, with no significant effect on polyguaiacol particle size or formation kinetics in solution. The effect of the sulfate in *method 2* experiments suggests the formation of heavier and more polydisperse particles in solution.

3. Characterization of Polymeric Particles Formed in Sulfate Solutions. *3a. Identification of Functional Groups Using ATR-FTIR.* To gain information about the chemical composition of the insoluble particles, ATR-FTIR measurements and TGA/DSC analyses were carried out. Figure 4a shows the ATR-FTIR absorbance spectrum of a polycatechol film of particles formed from a solution containing AS according to *method 2*. This spectrum was compared to the one we published earlier[23] and to the spectra of aqueous and solid phase ammonium sulfate (Figure 4e,f). The broad spectral feature between 1200 and 1000 cm^{-1} with peaks at 1100 and 1060 cm^{-1} was clearly due to the stretching mode of the sulfate groups.[44] This feature does not decrease in intensity with multiple cycles of washing with water suggesting that the sulfate groups are tightly bonded to the polycatechol particles.

The symmetry of these sulfate groups is lower than that of the free ions in solution.[45] The lower symmetry gives rise to wider peaks in the IR similar to what is observed for sulfate in

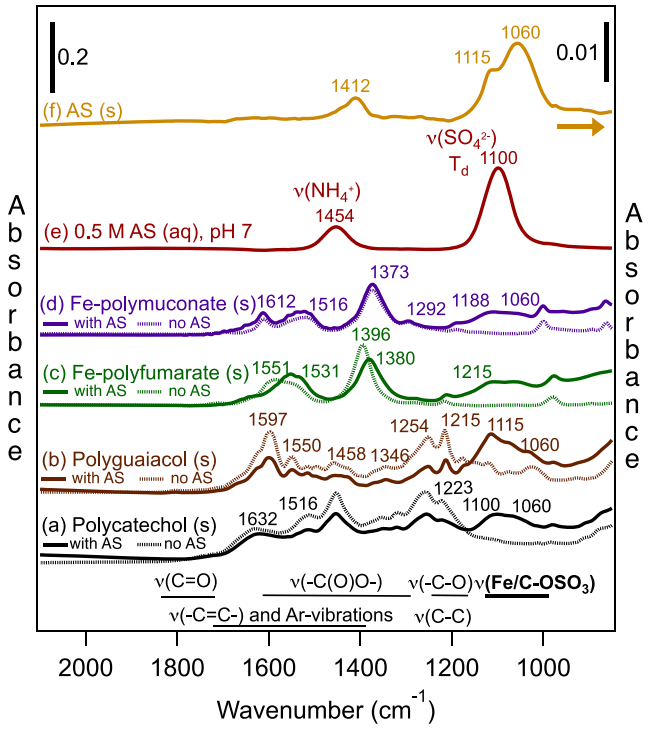

Figure 4. ATR-FTIR spectra of (a) solid polycatechol, (b) solid polyguaiacol, (c) solid Fe-polyfumarate, (d) solid Fe-polymuconate, (e) aqueous phase solution of ammonium sulfate (AS) at pH 7, and (f) solid AS. Solid and dashed lines in a–d are spectra collected for samples prepared with and without AS in solution according to *method 2*. Dashed spectra in parts a and b are from reference 23 and those in parts c and d are from reference 24.

solid AS (Figure 4f). There is no spectral evidence that the ammonium ion is present in these polymeric films. The sulfate absorption region in the spectrum of solid ammonium sulfate shows a more intense 1060 cm^{-1} peak relative to the 1115 cm^{-1} peak. However, the sulfate spectral features in Figure 4a for polycatechol with AS (solid line) show the opposite trend. This observation suggests that the bonding environment of the sulfate groups in polycatechol is different than that in solid AS. This result is expected as the sulfate anions are trapped in an organic polymer and not by the ammonium cation as in solid AS. For comparison, Figure 4b shows the ATR-FTIR absorbance spectrum of a polyguaiacol film of particles prepared in a solution containing ammonium sulfate according to *method 2* at pH 3. There is a clear spectral feature between 1200 and 1000 cm^{-1} with peaks at 1115 and 1060 cm^{-1} assigned to sulfate groups that is nonexistent in the spectrum we published earlier.[23] Similar to the case of the polycatechol particles prepared in a sulfate solution, multiple cycles of washings in water did not reduce the intensity of the sulfate spectral feature. In line with the product mass result in Figure 2b of polyguaiacol prepared according to *method 1* at pH 3, the ATR-FTIR absorbance spectrum of the dry film resembled that of the control spectrum in Figure 4b (i.e., no evidence of sulfate).

In addition, the ATR-FTIR absorbance spectrum of dry polyfumarate prepared in a sulfate solution according to *method 1* at pH 5 shows spectral features at 1110 and 1060 cm^{-1} assigned to $\nu(Fe\text{-}OSO_3)$ (Figure 4c). These results can be explained by either the sulfate trapped in the porous structure of Fe-polyfumarate[46] or the chelation of sulfate to

DOI: 10.1021/acs.est.9b00237
Environ. Sci. Technol. 2019, 53, 6708–6717

iron centers in the organometallic polymer due to ligand exchange with −OH or $-H_2O$ groups. Sulfate is an oxyanion and Apblet reported that the amorphous iron fumarate polymer is capable of binding oxyanions like phosphate and arsenate from water.[47] Hence, the increase in product mass observed in Figure 2f is very likely due to the additional mass of the sulfate groups rather than an increase in yield. The effect of sulfate on Fe-polymuconate product mass (Figures 2h and 1d) is not significantly different from the control values. As in the case with Fe-polyfumarate, the ATR-FTIR spectrum of dry Fe-polymuconate prepared in a sulfate solution according to *method 1* at pH 5 show features at 1110 and 1060 cm^{-1} assigned to $\nu(Fe\text{-}OSO_3)$ (Figure 4d). Because Fe-polymuconate does not have a porous structure, these sulfate features are likely due to ligand exchange with $-H_2O$ groups on the Fe centers in the polymer.

3b. Thermal Properties Using TGA/DSC. To further investigate the identity of the polycatechol particles formed from different procedures, Figure S4a,c shows the thermal decomposition and melting profile using TGA and DSC, respectively. The TGA data show that polycatechol particles prepared in sulfate solutions according to *method 1* and *2* start decomposing at ca. 250 °C, which is 150 °C lower than those prepared in control experiments. The DSC data shows that the melting of these particles starts earlier by 5−10 °C. For comparison, the TGA data in Figure S4b show that the thermal decomposition of the polyguaiacol particles prepared in sulfate solutions according to *method 2* starts earlier by 150 °C than the control particles and those prepared according to *method 1*. The melting behaviors of these particles in the DSC curve (Figure S4d) is not as clear as that of polycatechol but is different than the control particles and those prepared according to *method 1*.

The two major factors that cause shifts to lower temperatures in the TGA and DSC data of polymers and organic compounds are density and concentration of impurities. The effect of polymer density on the start temperature of thermal decomposition can be illustrated by examining the TGA curves of poly(methyl methacrylate) (PMMA)[48] and polytetrafluoroethylene (PTFE).[49] PMMA is more branched with a density of 1.19 g cm^{-3}, and it starts decomposing around 280 °C, while PTFE has a density of 2 g cm^{-3}, and it starts decomposing around 520 °C. Boyanov studied the thermal decomposition of metal sulfates in the presence of coke and found that mixtures started decomposing at temperatures that were 100−200 °C lower than those of the individual metal sulfates.[50] Plato and Glasgow showed that the percentage of impurities in organic compounds can be calculated from the melting point depression and heat of fusion obtained from their DSC curves.[51] Hence, it is very likely that the polycatechol particles formed in the presence of sulfate are also porous and can retain sulfate anions. In the case of polyguaiacol particles, their higher molecular weight (refer to the TGA curve in Figure S4b) and therefore higher viscosity[52] helps retain sulfate. This sulfate retention in polycatechol and polyguaiacol appears to take place during particle growth and hence contributes to their polydispersity and size.

The results presented herein have significant atmospheric environmental implications on our understanding of the fate of iron in aerosols with various degrees of atmospheric processing (e.g., reactive and unreactive partitioning of VOCs, heterogeneous oxidation, photodegradation,···). The formation of particles in solution presented herein suggests that a new amorphous insoluble solid phase will form in atmospheric aerosols containing the chemicals used in our studies. The low solubility of these particles makes them uniquely different from the much better known oligomeric compounds formed during VOC oxidation, which are commonly water-soluble.[27] The processes described herein will lead to liquid−solid phase separation, where the solid phase consists of the insoluble and strongly light-absorbing polycatechol, polyguaiacol, Fe-polyfumarate, and Fe-polymuconate. These inclusions will affect optical and hygroscopic properties of the aerosols. Images collected from field and lab studies on particles containing organic compounds, inorganic salts, and water reported different water uptake behavior for different morphologies that include homogeneous, core−shell, and partially engulfed mixing states.[52−54] Highly light-absorbing inclusions such as soot have been shown to affect the absorption and scattering coefficients of particles.[55] The novelty of our work is in uncovering metal-catalyzed processes leading to insoluble particle formation that complements the chemistry of soluble complexes of iron currently incorporated in atmospheric chemistry models.

These results also highlight the contrast in aqueous phase iron chemistry with atmospherically relevant organic compounds under dark versus irradiation conditions[25,56−59] (i.e., night versus daytime). The irradiated conditions result in the production of OH radicals that oxidize dissolved organics. In the presence of competing ligands for iron, dark solution reactions produce insoluble and colored particles from aromatic and aliphatic reagents. These reactions dominate over those that form soluble iron complexes. While results from *methods 1* and *2* were shown herein for comparison, *method 2* is more atmospherically relevant over a range of multicomponent aerosol processing. In addition, the results presented herein show a new role for oxalate in aerosol chemistry, given its higher concentrations than iron and organic reagents, which is to efficiently suppress secondary particle formation in solution. The trapping of sulfate in the organic polymers studied herein might result in changes in their hygroscopic properties and water uptake behavior reported recently[46] and their chemical and photochemical reactivities. These studies are currently underway in our laboratories.

■ ASSOCIATED CONTENT

Supporting Information

The Supporting Information is available free of charge on the ACS Publications website at DOI: 10.1021/acs.est.9b00237.

Detailed experimental procedures; chemicals; product mass experiments; HPLC, DLS, ATR-FTIR, ion chromatography, and TGA/DSC experiments; speciation curves; photographs of filters; schemes of suggested mechanisms; equilibrium constants; thermal decomposition and melting graphs (PDF)

■ AUTHOR INFORMATION

Corresponding Author

*Phone: (519)884-0710, ext. 2873. Fax: (519)746-0677. E-mail: halabadleh@wlu.ca.

ORCID

Sergey A. Nizkorodov: 0000-0003-0891-0052

Hind A. Al-Abadleh: 0000-0002-9425-0646

DOI: 10.1021/acs.est.9b00237
Environ. Sci. Technol. 2019, 53, 6708−6717

Author Contributions

[#]These coauthors contributed equally to the experimental work

Notes

The authors declare no competing financial interest.

■ ACKNOWLEDGMENTS

H.A.A. acknowledges partial funding from Laurier, NSERC, Canadian Foundation for Innovation, and the Fulbright Canada Research Chair in Atmospheric Chemistry, Air Quality and Climate Change program at the University of California Irvine. L.R. acknowledges funding from the NSERC Undergraduate Student Research Scholarship and Laurier Institute for Water Science Travel Undergraduate Student Scholarship programs. The authors thank Dr. Vladimir Kitaev (Laurier) for access to the DLS instrument, Sara Soldoozy at Laurier for guidance and training on Visual MINTEQ, v. 3.1 for the speciation equations, Nujhat Ali and Suki Gu at UCI for training LR on the DLS, and Henry Chin and Lauren Fleming for providing data on the solubility of particles at different pH. The authors thank Dr. Dmitry Fishman, the Director of the UCI Laser Spectroscopy Lab, for help with interpreting the DLS data, and Ralph Dickhout of the Analytical Chemistry Services at the University of Waterloo for the TGA/DSC data.

■ REFERENCES

(1) Farmer, D. K.; Cappa, C. D.; Kriedenweis, S. M. Atmospheric processes and their controlling influence on cloud condensation nuclei activity. *Chem. Rev.* **2015**, *115*, 4199−4217.

(2) Pöschl, U. Atmospheric aerosols: Compostion, transformation, climate and health effects. *Angew. Chem., Int. Ed.* **2005**, *44*, 7520−7540.

(3) Zhang, R.; Khalizov, A.; Wang, L.; Hu, M.; Xu, W. Nucleation and growth of nanoparticles in the atmosphere. *Chem. Rev.* **2012**, *112*, 1957−2011.

(4) Ziemann, P. J.; Atkinson, R. Kinetics, products, and mechanisms of secondary organic aerosol formation. *Chem. Soc. Rev.* **2012**, *41*, 6582−6605.

(5) Kanakidou, M.; Seinfeld, J. H.; Pandis, S. N.; Barnes, I.; Dentener, F. J.; Facchini, M. C.; Van Dingenen, R.; Ervens, B.; Nenes, A.; Nielsen, C. J.; Swietlicki, E.; Putaud, J. P.; Balkanski, Y.; Fuzzi, S.; Horth, J.; Moortgat, G. K.; Winterhalter, R.; Myhre, C. E. L.; Tsigaridis, K.; Vignati, E.; Stephanou, E. G.; Wilson, J. Organic aerosol and global climate modelling: A review. *Atmos. Chem. Phys.* **2005**, *5*, 1053−1123.

(6) Laskin, A.; Laskin, J.; Nizkorodov, S. A. Chemistry of atmospheric brown carbon. *Chem. Rev.* **2015**, *115*, 4335−4382.

(7) Al-Abadleh, H. A. A review on the bulk and surface chemistry of iron in atmospherically-relevant systems containing humic like substances. *RSC Adv.* **2015**, *5*, 45785−45811.

(8) Ito, A. Atmospheric processing of combustion aerosols as a source of bioavailable iron. *Environ. Sci. Technol. Lett.* **2015**, *2*, 70−75.

(9) Oakes, M.; Weber, R. J.; Lai, B.; Russell, A.; Ingall, E. D. Characterization of iron speciation in urban and rural single particles using XANES spectroscopy and micro x-ray fluorescence measurements: Investigating the relationship between speciation and fractional iron solubility. *Atmos. Chem. Phys.* **2012**, *12*, 745−756.

(10) Ault, A. P.; Peters, T. M.; Sawvel, E. J.; Casuccio, G. S.; Willis, R. D.; Norris, G. A.; Grassian, V. H. Single-particle SEM-EDX analysis of iron-containing coarse particulate matter in an urban environment: Sources and distribution of iron within Cleveland, Ohio. *Environ. Sci. Technol.* **2012**, *46*, 4331−4339.

(11) Guasco, T. L.; Cuadra-Rodriguez, L. A.; Pedler, B. E.; Ault, A. P.; Collins, D. B.; Zhao, D.; Kim, M. J.; Ruppel, M. J.; Wilson, S. C.; Pomeroy, R. S.; Grassian, V. H.; Azam, F.; Bertram, T. H.; Prather, K. A. Transition metal associations with primary biological particles in sea spray aerosol generated in a wave channel. *Environ. Sci. Technol.* **2014**, *48*, 1324−1333.

(12) Li, W.; Shao, L.; Shi, Z.; Chen, J.; Yuan, Q.; Yan, C.; Zhang, X.; Wang, Y.; Sun, J.; Zhang, Y.; Shen, X.; Wang, Z.; Wang, W. Mixing state and hygroscopicity of dust and haze particles before leaving asian continent. *J. Geophys. Res. Atmos.* **2014**, *119*, 1044−1059.

(13) Winton, V. H. L.; Edwards, R.; Bowie, A. R.; Keywood, M. D.; Williams, A. G.; Chambers, S. D.; Selleck, P. W.; Desservettaz, M.; Mallet, M. D.; Paton-Walsh, C. Dry season aerosol iron solubility in tropical Northern Australia. *Atmos. Chem. Phys.* **2016**, *16*, 12829−12848.

(14) Shi, Z. B.; Krom, M. D.; Jickells, T. D.; Bonneville, S.; Carslaw, K. S.; Mihalopoulos, N.; Baker, A. R.; Benning, L. G. Impacts on iron solubility in the mineral dust by processes in the source region and the atmosphere: A review. *Aeolian Res.* **2012**, *5*, 21−42.

(15) Srinivas, B.; Sarin, M.; Rengarajan, R. Atmospheric transport of mineral dust from the indo-gangetic plain: Temporal variability, acid processing, and iron solubility. *Geochem. Geophys. Geosyst.* **2014**, *15*, 3226−3243.

(16) Meskhidze, N.; Hurley, D.; Royalty, T. M.; Johnson, M. S. Potential effect of atmospheric dissolved organic carbon on the iron solubility in seawater. *Mar. Chem.* **2017**, *194*, 124−132.

(17) Johnson, M. S.; Meskhidze, N.; Solmon, F.; Gasso, S.; Chuang, P. Y.; Gaiero, D.; Yantosca, R. M.; Wu, S.; Wang, Y.; Carouge, C. Modeling dust and soluble iron deposition to the South Atlantic Ocean. *J. Geophys. Res.* **2010**, *115*, D15202.

(18) Shi, Z.; Krom, M. D.; Bonneville, S.; Benning, L. G. Atmospheric processing outside clouds increases soluble iron in mineral dust. *Environ. Sci. Technol.* **2015**, *49*, 1472−1477.

(19) Ingall, E. D.; Feng, Y.; Longo, A. F.; Lai, B.; Shelley, R. U.; Landing, W. M.; Morton, P. L.; Nenes, A.; Mihalopoulos, N.; Violaki, K.; Gao, Y.; Sahai, S.; Castorina, E. Enhanced iron solubility at low pH in global aerosols. *Atmosphere* **2018**, *9*, 201−218.

(20) Ito, A.; Shi, Z. Delivery of anthropogenic bioavailable iron from mineral dust and combustion aerosols to the ocean. *Atmos. Chem. Phys.* **2016**, *16*, 85−99.

(21) Shi, G. L.; Xu, J.; Peng, X.; Xiao, Z.; Chen, K.; Tian, Y.; Guan, X.; Feng, Y.; Yu, H.; Nenes, A.; Russell, A. pH of aerosols in a polluted atmosphere: Source contributions to highly acidic aerosol. *Environ. Sci. Technol.* **2017**, *51*, 4289−4296.

(22) Nguyen, T. K. V.; Zhang, Q.; Jimenez, J. L.; Pike, M.; Carlton, A. G. Liquid water: Ubiquitous contributor to aerosol mass. *Environ. Sci. Technol. Lett.* **2016**, *3*, 257−263.

(23) Slikboer, S.; Grandy, L.; Blair, S. L.; Nizkorodov, S. A.; Smith, R. W.; Al-Abadleh, H. A. Formation of light absorbing soluble secondary organics and insoluble polymeric particles from the dark reaction of catechol and guaiacol with Fe(III). *Environ. Sci. Technol.* **2015**, *49*, 7793−7801.

(24) Tran, A.; William, G.; Younus, S.; Ali, N. N.; Blair, S. L.; Nizkorodov, S. A.; Al-Abadleh, H. A. Efficient formation of light-absorbing polymeric nanoparticles from the reaction of soluble Fe(III) with C4 and C6 dicarboxylic acids. *Environ. Sci. Technol.* **2017**, *51*, 9700−9708.

(25) Arroyo, P. C.; Malecha, K. T.; Ammann, M.; Nizkorodov, S. A. Influence of humidity and iron(III) on photodegradation of atmospheric secondary organic aerosol particles. *Phys. Chem. Chem. Phys.* **2018**, *20*, 30021−30031.

(26) Craig, R. L.; Nandy, L.; Axson, J. L.; Dutcher, C. S.; Ault, A. P. Spectroscopic determination of aerosol pH from acid−base equilibria in inorganic, organic, and mixed systems. *J. Phys. Chem. A* **2017**, *121*, 5690−5699.

(27) Tolocka, M. P.; Jang, M.; Ginter, J. M.; Cox, F. J.; Kamens, R. M.; Johnston, M. V. Formation of oligomers in secondary organic aerosol. *Environ. Sci. Technol.* **2004**, *38*, 1428−1434.

(28) Kundu, S.; Kawamura, K.; Andreae, T. W.; Hoffer, A.; Andreae, M. O. Molecular distributions of dicarboxylic acids, ketocarboxylic acids and α-dicarbonyls in biomass burning aerosols: Implications for photochemical production and degradation in smoke layers. *Atmos. Chem. Phys.* **2010**, *10*, 2209−2225.

DOI: 10.1021/acs.est.9b00237
Environ. Sci. Technol. 2019, 53, 6708−6717

(29) Zhao, R.; Lee, A. K. Y.; Abbatt, J. P. D. Investigation of aqueous-phase photooxidation of glyoxal and methylglyoxal by aerosol chemical ionization mass spectrometry: Observation of hydroxyhydroperoxide formation. *J. Phys. Chem. A* **2012**, *116* (24), 6253−6263.
(30) Zhang, G.; Lin, Q.; Peng, L.; Yang, Y.; Jiang, F.; Liu, F.; Song, W.; Chen, D.; Cai, Z.; Bi, X.; Miller, M.; Tang, M.; Huang, W.; Wang, X.; Peng, P.; Sheng, G. Oxalate formation enhanced by Fe-containing particles and environmental implications. *Environ. Sci. Technol.* **2019**, *53*, 1269−1277.
(31) Paris, R.; Desboeufs, K. Effect of atmospheric organic complexation on iron-bearing dust solubility. *Atmos. Chem. Phys.* **2013**, *13*, 4895−4905.
(32) Gonzalez, M. C.; Roman, E. S., Environmental photochemistry in heterogeneous media. In *Hdb environmental chemistry*; Springer-Verlag: Berlin, 2005; Vol. 2, pp 49−75.
(33) Hennigan, C. J.; Izumi, J.; Sullivan, A. P.; Weber, R. J.; Nenes, A. A critical evaluation of proxy methods used to estimate the acidity of atmospheric particles. *Atmos. Chem. Phys.* **2015**, *15*, 2775−2790.
(34) Yu, J. Z.; Huang, X.-F.; Xu, J.; Hu, M. When aerosol sulfate goes up, so does oxalate: Implication for the formation mechanisms of oxalate. *Environ. Sci. Technol.* **2005**, *39*, 128−133.
(35) Bikkina, S.; Kawamura, K.; Sarin, M. Secondary organic aerosol formation over coastal ocean: Inferences from atmospheric water-soluble low molecular weight organic compounds. *Environ. Sci. Technol.* **2017**, *51*, 4347−4357.
(36) Lide, D. R. *CRC handbook of chemistry and physics*; Taylor & Francis: Boca Raton, 2012−2013; Vol. 93.
(37) Ragnar, M.; Lindgren, C. T.; Nilvebrant, N. O. pKa-values of guaiacyl and syringyl phenols related to lignin. *J. Wood Chem. Technol.* **2000**, *20*, 277−305.
(38) Faure, E.; Falentin-Daudre, C.; Jerome, C.; Lyskawa, J.; Fournier, D.; Woisel, P.; Detrembleur, C. Catechols as versatile platforms in polymer chemistry. *Prog. Polym. Sci.* **2013**, *38*, 236−270.
(39) Perron, N. R.; Brumaghim, J. L. A review of the antioxidant mechanisms of polyphenol compounds related to iron binding. *Cell Biochem. Biophys.* **2009**, *53*, 75−100.
(40) Park, J. S. B.; Wood, P. M.; Davies, M. J.; Gilbert, B. C.; Whitwood, A. C. A kinetic and esr investigation of iron(II) oxalate oxidation by hydrogen peroxide and dioxygen as a source of hydroxyl radicals. *Free Radical Res.* **1997**, *27*, 447−458.
(41) Hwang, S.; Lee, C.-H.; Ahn, I.-S. Product identification of guaiacol oxidation catalyzed by manganese peroxidase. *J. Ind. Eng. Chem.* **2008**, *14*, 487−492.
(42) Doerge, D. R.; Divi, R. L.; Churchwell, M. I. Identification of the colored guaiacol oxidation product produced by peroxidases. *Anal. Biochem.* **1997**, *250*, 10−17.
(43) Crawford, R. L.; Robinson, L. E.; Foster, R. D. Polyguaiacol: A useful model polymer for lignin biodegradation research. *Arch. Microbiol.* **1981**, *41*, 1112−1116.
(44) Miller, F. A.; Wilkins, C. H. Infrared spectra and characteristic frequencies of inorganic ions. *Anal. Chem.* **1952**, *24*, 1253−1294.
(45) Hug, S. J. In situ fourier transform infrared measurements of sulfate adsorption on hematite in aqueous solutions. *J. Colloid Interface Sci.* **1997**, *188*, 415−422.
(46) Rahman, M. A.; Al-Abadleh, H. A. Surface water structure and hygroscopic properties of light absorbing secondary organic polymers of atmospheric relevance. *ACS Omega* **2018**, *3*, 15519−15529.
(47) Apblett, A. W. Iron coordination polymers for adsorption of arsenate and phosphate. 2013, U.S. Patent US2013/0292338 A1, 1−8.
(48) Nyambo, C.; Songtipya, P.; Manias, E.; Jimemez-Gasco, M. M.; Wilkie, C. A. Effect of mgal-layered double hydroxide exchanged with linear alkyl carboxylates on fire-retardancy of PMMA and PS. *J. Mater. Chem.* **2008**, *18*, 4827−4838.
(49) Pan, C.; Kou, K.; Jia, Q.; Zhang, Y.; Guanglei, W.; Ji, T. Improved thermal conductivity and dielectric properties of HBN/PTFE composites via surface treatment by silane coupling agent. *Composites, Part B* **2017**, *111*, 83−90.
(50) Boyanov, B. S. DTA and TGA study of $MeSO_4$ (Me = Fe, Co, Ni) dissociation in the presence of coke. *J. Min. Metall., Sect. B* **2002**, *38*, 103−116.
(51) Plato, C.; Glasgow, A. R. Differential scanning calorimetry as a general method for determining the purity and heat of fusion of high-purity organic chemicals. Application to 95 compounds. *Anal. Chem.* **1969**, *41*, 330−336.
(52) Koop, T.; Bookhold, J.; Shiraiwa, M.; Pöschl, U. Glass transition and phase state of organic compounds: Dependency on molecular properties and implications for secondary organic erosols in the atmosphere. *Phys. Chem. Chem. Phys.* **2011**, *13*, 19238−19255.
(53) Freedman, M. A. Phase separation in organic aerosol. *Chem. Soc. Rev.* **2017**, *46*, 7694−7705.
(54) Song, M.; Marcolli, C.; Krieger, U. K.; Lienhard, D. M.; Peter, T. Morphologies of mixed organic/inorganic/aqueous aerosol droplets. *Faraday Discuss.* **2013**, *165*, 289−316.
(55) Liu, D.; Whitehead, J.; Alfarra, M. R.; Reyes-Villegas, E.; Spracklen, D. V.; Reddington, C. L.; Kong, S.; Williams, P. I.; Ting, Y.-C.; Haslett, S.; Taylor, J. W.; Flynn, M. J.; Morgan, W. T.; McFiggans, G.; Coe, H.; Allan, J. D. Black-carbon absorption enhancement in the atmosphere determined by particle mixing state. *Nat. Geosci.* **2017**, *10*, 184−188.
(56) Thomas, D. A.; Coggon, M. M.; Lignell, H.; Schilling, K. A.; Zhang, X.; Schwantes, R. H.; Flagan, R. C.; Seinfeld, J. H.; Beauchamp, J. L. Real-time studies of iron oxalate-mediated oxidation of glycolaldehyde as a model for photochemical aging of aqueous tropospheric aerosols. *Environ. Sci. Technol.* **2016**, *50*, 12241−12249.
(57) George, C.; Ammann, M.; D'Anna, B.; Donaldson, D. J.; Nizkorodov, S. A. Heterogeneous photochemistry in the atmosphere. *Chem. Rev.* **2015**, *115*, 4218−4258.
(58) George, C.; D'Anna, B.; Herrmann, H.; Weller, C.; Vaida, V.; Donaldson, D. J.; Bartels-Rausch, T.; Ammann, M., Emerging areas in atmospheric photochemistry. In *Atmospheric and aerosol chemistry*, McNeill, V. F.; Ariya, P. A., Eds.; Springer: Heidelberg, 2012; Vol. 339, pp 1−54.
(59) Pang, H.; Zhang, Q.; Wang, H.; Cai, D.; Ma, Y.; Li, L.; Li, K.; Lu, X.; Chen, H.; Yang, X.; Chen, J. Photochemical aging of guaiacol by Fe(III)−oxalate complexes in atmospheric aqueous phase. *Environ. Sci. Technol.* **2019**, *53*, 127−136.

DOI: 10.1021/acs.est.9b00237
Environ. Sci. Technol. 2019, 53, 6708−6717